Environmental Science & Technology

Article

pubs.acs.org/est

Aggregation Behavior of Dissolved Black Carbon: Implications for Vertical Mass Flux and Fractionation in Aquatic Systems

Fanchao Xu,[†] Chenhui Wei,[†] Qingqing Zeng,[†] Xuening Li,[‡] Pedro J.J. Alvarez,[§] Qilin Li,[§] Xiaolei Qu,[*,†] and Dongqiang Zhu[∥]

[†]State Key Laboratory of Pollution Control and Resource Reuse, School of the Environment, Nanjing University, Jiangsu 210023, China

[‡]State Key Laboratory of Petroleum Pollution Control, CNPC Research Institute of Safety and Environmental Technology, Beijing 102206, China

[§]Department of Civil and Environmental Engineering, Rice University, Houston Texas 77005, United States

[∥]School of Urban and Environmental Sciences, Peking University, Beijing 100871, China

Supporting Information

ABSTRACT: The fluvial export of dissolved black carbon (DBC) is a major land-ocean flux in the global black carbon cycle, affecting the size of refractory carbon pool in the oceans. The aggregation behavior of DBC is a significant determinant of its transport and vertical mass flux. In this study, the aggregation kinetics and interaction energy of DBC leached from biochar were investigated. DBC was mainly stabilized by hydration force and underwent structural compacting in divalent cation solutions. Na^+ and Mg^{2+} had limited impact on the colloidal stability of DBC due to the strong hydration of these cations. Ca^{2+} and Ba^{2+} readily destabilized DBC by forming inner-sphere complexes, reducing its hydrophilicity. Consistently, charge reversal of DBC was observed with high concentrations of Ca^{2+} and Ba^{2+}. Simulated sunlight exposure led to photo-oxidation of DBC, increasing its colloidal stability. DBC behaved nonconservatively in laboratory mixing experiments using estuary water samples due to aggregation/sedimentation; while model aquatic humic acid behaved conservatively. Our results infer that there is a vertical mass flux of DBC and possible fractionation from the dissolved organic matter pool in the fluvial and estuarine systems, which have been overlooked in efforts to determine global carbon budgets and associated climate change implications.

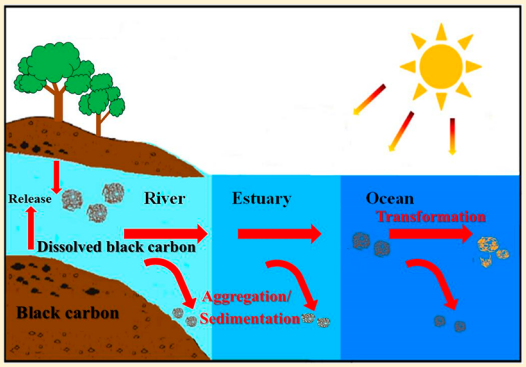

INTRODUCTION

Black carbon is the carbonaceous residue formed during incomplete combustion of biomass or fossil fuel.[1] It can release the water-soluble fraction, usually referred to as dissolved black carbon (DBC), when in contact with water during infiltration or surface runoff of stormwater, which comprises around 10% of the dissolved organic carbon (DOC) in the rivers and 2% in the oceans.[2−6] Global fluvial discharge of DBC is estimated to be about 26.5 million tons per year, being the major flux of black carbon to the oceans.[5] Owing to the recalcitrant nature of DBC, this flux is an important contributor to the oceanic pool of refractory carbon, which plays a significant role in oceanic carbon cycling, atmospheric CO_2 levels, and climate change.[2,5−8] Furthermore, DBC contains abundant aromatic domains and oxygen-containing functional groups,[3,4] making it a good sorbent for organic compounds and metals. Thus, it can serve as a carrier for priority pollutants,[9] affecting their fate and transport.

The rate and extent of aggregation of DBC and subsequent formation of fast-settling particles in fluvial systems can significantly affect its flux to the oceans, influencing the global budget of refractory carbon, its impact on climate change, and the environmental fate of priority contaminants. However, little is known about the aggregation behavior and vertical mass flux of DBC in aquatic systems. Two previous studies investigated the deposition behavior of DBC in the saturated granular media,[10,11] and described the deposition behavior adequately using the extended Derjaguin−Landau−Verwey−Overbeek (XDLVO) theory to consider electrostatic and Lewis acid-base interactions between DBC and quartz sand.[10] The presence of humic acid was reported to enhance the transport of DBC in sand columns, while iron oxyhydroxide coatings on sand grains decreased DBC transport.[11] Nevertheless, the aggregation behavior of DBC has not been addressed in the literature. Furthermore, DBC was reported to undergo structural changes during solar irradiation,[3,12−14] and the

Received: August 17, 2017
Revised: November 8, 2017
Accepted: November 13, 2017
Published: November 13, 2017

DOI: 10.1021/acs.est.7b04232
Environ. Sci. Technol. 2017, 51, 13723−13732

impact of solar exposure on DBC aggregation behavior is still unknown.

The removal of DOM from aquatic systems is determined by its degradation or aggregation into large particulates.[15] Several studies have reported that the riverine DOM pool is transported conservatively (i.e., without addition or loss) to the oceans.[16−18] On the other hand, several studies pointed out that DOM behaves nonconservatively in several estuaries due to multiple biogeochemical processes including aggregation/sedimentation, degradation, autochthonous production, and solute-particle interactions.[19−21] The vertical mass flux of DBC was largely unaccounted for in the current estimation of its land-ocean flux.[2,5,8,22] The nonconservative behavior of DBC due to aggregation/sedimentation may potentially result in the fractionation of DBC from the DOM pool and its accumulation in terrestrial sediments as important intermediate pools, which has not been addressed yet.

In the present study, DBC leached from biomass-derived black carbon was used as a proxy for DBC in natural aquatic systems.[3,12] It is a continuum of macromolecules with high aromaticity, which is different from black carbon nanoparticles generated by ball-milling in a previous study.[4,12,23] The initial aggregation kinetics and electrokinetic properties of DBC were characterized in the presence of naturally abundant mono- and divalent cations, including Na^+, Mg^{2+}, Ca^{2+}, and Ba^{2+}. The interaction energy of London-van der Waals force, electrostatic force, and Lewis acid-base interactions was calculated based on the XDLVO model. The impact of solar exposure on its structural properties and aggregation behavior was also examined. The behavior of DBC during mixing of natural water samples collected from two end-members in the Yangtze River Estuary was compared with a theoretical conservative mixing scenario to discern the significance of nonconservative processes (i.e., aggregation/sedimentation in this case). Our main objectives were to (1) determine the effect of ionic strength, ionic composition, and sunlight exposure on the aggregation behavior of DBC; (2) discern the aggregation mechanisms; and (3) examine possible vertical mass flux and fractionation of DBC along the salinity gradient due to aggregation/sedimentation processes, which are important knowledge gaps to inform global black carbon budgets and associated climate change implications.

MATERIALS AND METHODS

Materials. $CaCl_2$ (>99%) was obtained from Alfa Aesar, UK. $MgCl_2$ (>99.5%), NaCl (>99.5%), and $BaCl_2$ (>99%) were purchased from Sigma-Aldrich. Deuteroxide (D_2O, 99.8 atom % D) was purchased from Tokyo Chemical Industry, Japan. Sodium-3-trimethylsilyl propionate (TMSP-2,2,3,3-D4) was purchased from Cambridge Isotope Laboratories, USA. Suwannee River humic acid (SRHA) was provided by the International Humic Substances Society (IHSS, St. Paul, MN). Deionized water (18.2 MΩ·cm resistivity at 25 °C) used in the experiments was produced by an ELGA Labwater system (PURELAB Ultra, ELGA LabWater Global Operations, UK).

Preparation of DBC. DBC was released from bulk black carbon by gentle sonication in water as described in a previous study.[3] Briefly, bamboo shavings collected from Lishui, Zhejiang Province, China was pulverized into powder (high-speed pulverizer FW 100, Tianjin Taisite Instrument, China) and pyrolyzed in a muffle furnace under oxygen-limited condition. The pyrolysis temperature was set to increase from 20 to 400 °C in 2 h and kept at 400 °C for 3 h. The resulting black carbon was pulverized and passed through a 100-mesh sieve. The sieved black carbon powder (30 g) was mixed with 500 mL deionized water in a 1000 mL glass beaker; sonicated in a sonication bath (KH-800TDB, Kunshan Hechuang Ultrasonic Instrument, China) at 50 W for 30 min; and filtered through a 0.45 μm membrane (Pall). The residue retained on the membrane was collected and subjected to another round of sonication and filtration. The sonication-filtration cycle was repeated three times. The filtrate from each cycle was collected and freeze-dried to yield DBC powder, which was stored in a desiccator at room temperature until use. The DBC stock solution was made by dissolving the DBC powder in deionized water. The pH of the stock solution was adjusted to 6.8 using HCl.

Irradiation Experiments. DBC solution was irradiated with simulated sunlight to examine the impact of sunlight exposure on the colloidal stability of DBC. A xenon lamp (CEL-HXF300, AULTT, China) was used to simulate the solar irradiation. The lamp spectrum was similar to natural sunlight as measured by a spectrometer (USB2000+, Ocean Optics, FL) (Supporting Information (SI) Figure S1). The DBC solution (20 mL, 100 mg/L) was stirred at 200 rpm in a 50 mL glass vial which was immersed in a water-circulating bath at 20 ± 0.1 °C. The DBC solution was irradiated by the xenon lamp from the top at a distance of 0.2 m for 24 and 48 h, respectively. Water loss due to evaporation during the experiment was compensated using deionized water.

Aggregation Kinetics of DBC. *Measurement of Particle Aggregation Rate.* The aggregation kinetics of the original and irradiated DBC were studied in various solution chemistry by time-resolved dynamic light scattering (DLS) measurements using a ZEN 3500 Zetasizer Nano ZS (Malvern, Worcestershire, UK) equipped with a 532 nm laser. The refractive index of DBC was set to be 2.20.[24] The DBC stock solution was sonicated in a sonication bath at 50 W for 5 min before the aggregation experiments. In the measurements of aggregation kinetics, 0.2 mL of 100 mg/L DBC solution and a predetermined amount of electrolyte stock solution and deionized water were introduced into a disposable polystyrene cuvette (Sarstedt, Germany) to yield a sample with a total volume of 1 mL. The sample was briefly mixed and immediately analyzed at 25 °C. The time-resolved DLS measurements monitor the average hydrodynamic diameter of DBC with the autocorrelation function being accumulated over a period of 7 s. If the particle size increased or decreased more than 50% in 7 s, the measurement was removed from the data set.

Determination of Aggregation Kinetics. The initial aggregation rate of DBC was determined by applying linear least-squares regression to the $d_h(t)$ data from the initial value $d_h(0)$ to 1.5 $d_h(0)$. The attachment efficiency α is a key matric to quantify the tendency of particle aggregation in a given water chemistry. It was determined by normalizing the initial aggregation rate in the solution of interest by that in the diffusion-limited regime.[25,26] Stability curves of DBC were drawn by plotting the α value as a function of the electrolyte concentration. The initial aggregation rate in the diffusion-limited regime was the average of the initial aggregation rates at the plateau of the stability curve. The critical coagulation concentration (CCC) was approximated by the electrolyte concentration where the diffusion-limited regime was achieved.

DOI: 10.1021/acs.est.7b04232
Environ. Sci. Technol. 2017, 51, 13723−13732

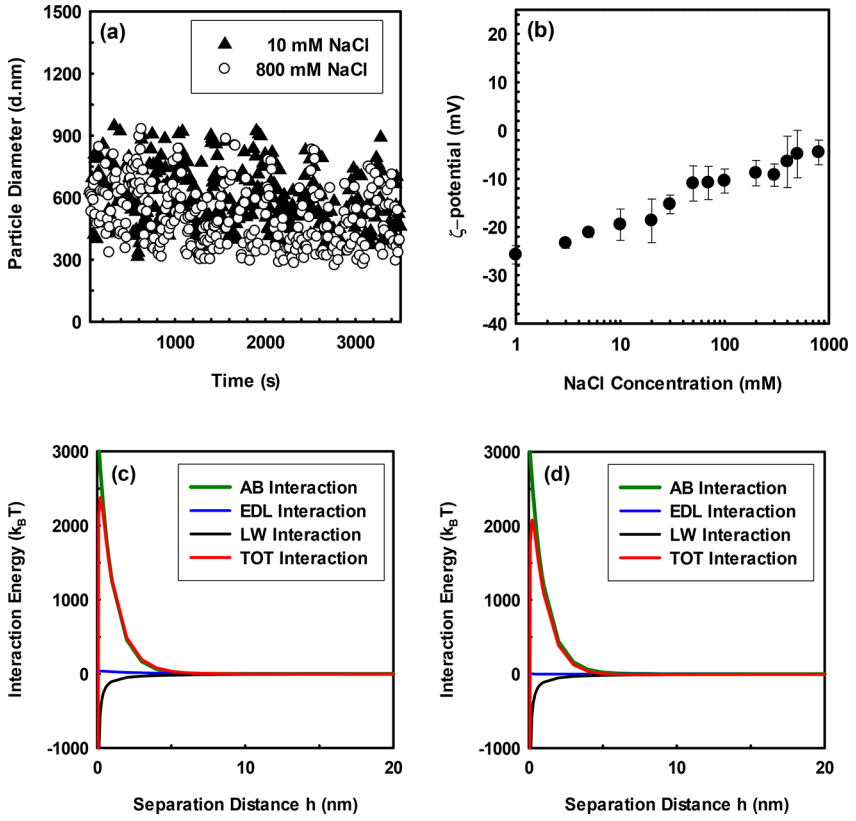

Figure 1. (a) Aggregation profile of 20 mg/L DBC in 10 and 800 mM NaCl solutions at pH 6.5 ± 0.4 measured by time-resolved dynamic light scattering; (b) ζ-potential of DBC as a function of NaCl concentration. Error bar represents one standard deviation of five measurements. The interaction energy of London-van der Waals force (LW), electrostatic force (EDL), Lewis acid-base interactions (AB), and the total interaction energy (TOT) of DBC in (c) 10 mM and (d) 800 mM NaCl solutions.

Characterization of DBC. Transmission electron microscope (TEM) images of DBC were taken using a JEM-200CX, JEOL, Japan.

Electrokinetic Properties of DBC. The electrophoretic mobility (EPM) and ζ-potential of DBC in different solution chemistry were measured by phase analysis light scattering (PALS) using the ZEN 3500 Zetasizer Nano ZS (Malvern, Worcestershire, UK). Each sample was measured five times at 25 °C in a folded capillary cell (Malvern, Worcestershire, UK).

Contact Angle Measurements. The DBC solution with different water chemistry was filtered through an ultrafiltration membrane (3 kDa, Millipore Corporation) using an ultrafiltration cell (model 8010, Millipore Corporation) to form a DBC layer on the membrane. The DBC layer on top of the ultrafiltration membrane was dried by nitrogen gas under room temperature and then subjected to static contact angle measurements. Static contact angles of probe liquids including water, glycerol, and *n*-decane on the surface of DBC layer were measured at least three times at different locations by an optical contact angle measuring device (OCA30, Dataphysics Instruments Gmb, Germany).

Proton Nuclear Magnetic Resonance (^{1}H NMR) Analysis. Ten milliliters of 1000 mg/L DBC in D_2O was irradiated using the same setting as irradiation experiments. Samples were withdrawn from the reactor at predetermined irradiation time and analyzed by NMR spectroscopy. The ^{1}H NMR spectra were acquired on a Bruker AVANCE DRX-600 NMR spectrometer (Bruker, MA). The chemical shifts (δ, ppm) were internally referenced to a standard, TMSP-2,2,3,3-D4.

Water Sample Collection and Mixing Experiments. The freshwater sample was collected from Yangtze River near Shanghai (N 31°33.143′, E 121°44.645′). The seawater sample was collected from the beach at Gouqi Island in the East China Sea (N 30°43.176′, E 122°47.573′). Both water samples were filtered through 0.45 μm membranes (Pall) after collected. To investigate the estuarine mixing behavior of DBC, the laboratory mixing experiments were carried out using these two water samples as the end-members of Yangtze River Estuary. Two milligrams of DBC or SRHA was dissolved in 200 mL freshwater sample to simulate a high-DBC/SRHA-containing river water. It was mixed with the seawater sample in different proportions to form a salinity gradient. The resulting mixtures were kept quiescent for 24 h in the dark. The absorption spectra of the mixtures after 24 h settling were measured by UV−vis spectroscopy in a 1 cm quartz cuvette. The absorption coefficient at 254 nm, a_{254}, was used to quantify the abundance of DBC/SRHA in water samples.[22]

RESULT AND DISCUSSION

Characterization of DBC. DBC forms a stable solution of brown color in deionized water. TEM images suggest that DBC assembles into irregular-shaped particles with diameters of hundreds of nanometers (SI Figure S2). It was negatively charged with a ζ-potential of −25.8 ± 1.9 mV (i.e., electrophoretic mobility of $-1.8 \pm 0.1 \times 10^{-8}$ m^2 V^{-1} s^{-1}) in 1 mM NaCl solution at pH 6.85. This is lower than the ζ-potential of DBC released from black carbon made from the slow pyrolysis of pine needle and wheat straw, −28.9 ∼ −36.6 mV.[10,11] The elemental and structural properties of DBC were

DOI: 10.1021/acs.est.7b04232
Environ. Sci. Technol. 2017, 51, 13723−13732

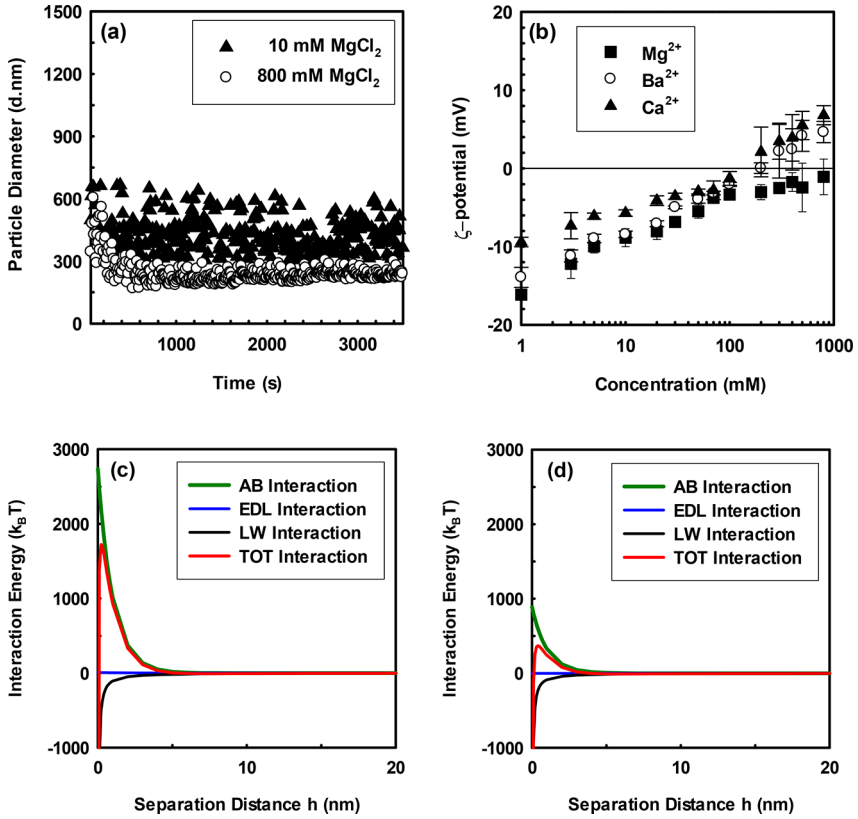

Figure 2. (a) Aggregation profile of 20 mg/L DBC in 10 and 800 mM $MgCl_2$ solutions at pH 6.2 ± 0.5 measured by time-resolved dynamic light scattering; (b) ζ-potential of DBC as a function of $MgCl_2$, $CaCl_2$, and $BaCl_2$ concentration. Error bar represents one standard deviation of five measurements. The interaction energy of London-van der Waals force (LW), electrostatic force (EDL), Lewis acid-base interactions (AB), and the total interaction energy (TOT) of DBC in (c) 10 mM and (d) 800 mM $MgCl_2$ solutions.

thoroughly characterized in our previous studies.[3,4] The (O+N)/C ratio of DBC was 0.66, slightly higher than SRHA, a reference humic acid from the International Humic Substances Society, 0.62.[4,27] DBC used in this work contains 43.7% aromatic carbon, 32.4% carboxyl/ester/quinone carbon, 5.5% aromatic C−O carbon, and 18.5% aliphatic carbon as determined by quantitative solid-state ^{13}C NMR.[3] It has more carboxyl/ester/quinone and aromatic carbons, but less aliphatic carbon than SRHA.[3,25] The elemental and structural analyses suggest the abundance of polar moieties, especially carboxyl groups, in DBC. Note that DBC in this study refers to all carbon leached from biomass-derived black carbon. It contains a wider range of carbon materials than that in previous spatiotemporal distribution studies which considered DBC as only highly condensed aromatic structures in the DOM pool.[2,28,29]

Aggregation Behavior of DBC in Monovalent Cation Solutions. The aggregation kinetics of DBC in 10 mM and 800 mM NaCl solutions are shown in Figure 1a. There was no significant change of hydrodynamic size of DBC within 1 h with NaCl concentrations up to 800 mM, which was higher than most ionic strength found in natural aquatic systems. Classical DLVO theory points out that the thermodynamics of particle attachment is controlled by the interplay of London-van der Waals force and electrostatic force;[30,31] and the aggregation behavior is mostly decided by the surface charge as reflected by the electrokinetic properties.[32−34] The ζ-potential of DBC was examined over a wide range of NaCl concentrations as shown in Figure 1b. DBC became less negatively charged from −25.8 ± 1.9 mV to −4.5 ± 2.6 mV as the NaCl concentration increased from 1 mM to 800 mM owing to charge screening. In the 800 mM NaCl solution, the ζ-potential of DBC was −4.5 ± 2.6 mV, close to neutral. Thus, electrostatic repulsion alone cannot account for the strong colloidal stability of DBC (i.e., its ability to resist aggregation). We further examined the aggregation behavior of DBC in the framework of XDLVO theory. The interaction energy of London-van der Waals force, electrostatic force, Lewis acid-base interactions, and the total interaction energy of DBC particles in 10 mM and 800 mM NaCl solutions were summarized in Figure 1c and 1d (see detailed calculation[35,36] and data set in SI). The free energy of Lewis acid-base interactions between DBC particles (G^{AB}) was determined using contact angle measurements and Young-Dupré equation.[10,35] The calculated ΔG^{AB} were 37.3 mJ m^{-2} and 35.7 mJ m^{-2} in 10 mM and 800 mM NaCl solutions respectively, indicating the strong hydrophilic nature of DBC particle surfaces.[35] This is consistent with the high polarity index (i.e., (O+N)/C ratio) and the abundant oxygen-containing functional groups of DBC. The positive nature of ΔG^{AB} also suggests repulsive forces between DBC particles due to surface cohesion water, that is, hydration force.[35,37] Clearly, the hydration force played a predominant role in the stabilization of DBC at both low and high NaCl concentrations (Figure 1c and d). The aggregation behavior of DBC is different from black carbon nanoparticles which can be destabilized by Na^+ with a CCC of 250 mM,[23] consistent with its macromolecular nature.

Aggregation Behavior of DBC in Divalent Cation Solutions and Charge Reversal. Colloidal stability depends strongly on the valence of counterions, as described by the

DOI: 10.1021/acs.est.7b04232
Environ. Sci. Technol. 2017, 51, 13723−13732

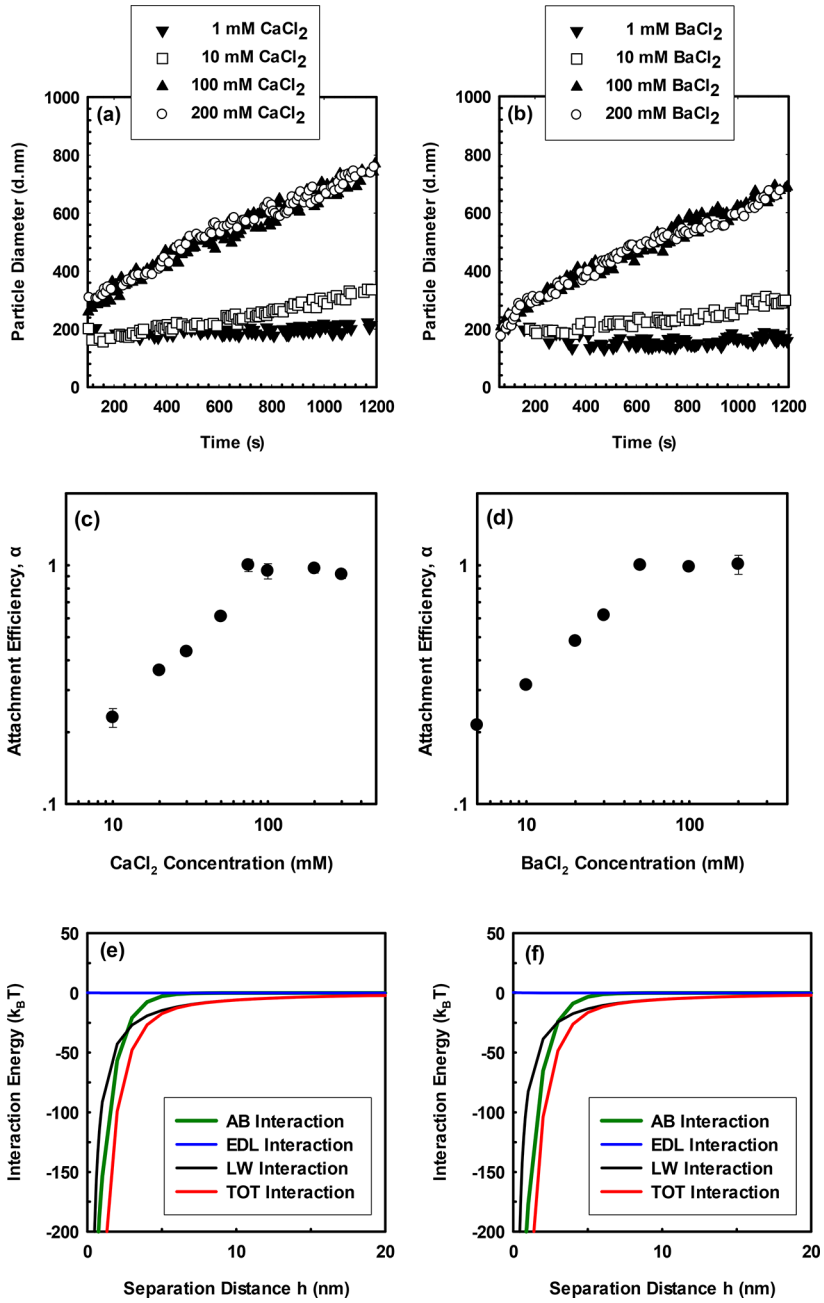

Figure 3. Aggregation profile of 20 mg/L DBC in (a) $CaCl_2$ and (b) $BaCl_2$ solutions at pH 6.0 ± 0.5 measured by time-resolved dynamic light scattering; and attachment efficiencies of DBC as a function of (c) $CaCl_2$ concentration and (d) $BaCl_2$ concentration. The interaction energy of London-van der Waals force (LW), electrostatic force (EDL), Lewis acid-base interactions (AB), and the total interaction energy (TOT) of DBC in 100 mM (e) $CaCl_2$ and (f) $BaCl_2$ solutions.

Schulze-Hardy Rule.[38] Mg^{2+}, Ca^{2+}, and Ba^{2+} are divalent cations found in natural waters, which are expected to impact the colloidal stability of DBC more significantly than monovalent cations. The aggregation kinetics of DBC in 10 mM and 800 mM $MgCl_2$ solutions are shown in Figure 2a. The particle size of DBC decreased in the initial stage after mixing with $MgCl_2$ solutions and then stabilized at 422.7 ± 77.3 nm and 229.2 ± 22.4 nm in 10 mM and 800 mM $MgCl_2$ solutions, respectively. DBC contains abundant carboxyl and phenolic groups, providing electrostatic repulsion between functional moieties and consequently leads to a stretched configuration. The presence of Mg^{2+} reduced the intramolecular electrostatic repulsion, resulting in a more compact configuration of DBC. Thus, the initial decrease in particle size can be attributed to structural compacting, which was previously observed for DOM and polyelectrolytes.[39−41] No significant aggregation was observed in 800 mM $MgCl_2$ solution in 1 h. The XDLVO model calculation of the interaction energy of DBC in 10 mM and 800 mM $MgCl_2$ solutions is present in Figure 2c and d. The high colloidal stability of DBC in $MgCl_2$ solutions is consistent with the high energy barrier provided by hydration force.

In contrast to that observed in NaCl and $MgCl_2$ solutions, Ca^{2+} and Ba^{2+} can readily induce the aggregation of DBC. Representative aggregation profiles of DBC in $CaCl_2$ and $BaCl_2$ solutions are present in Figure 3a and b. The attachment

DOI: 10.1021/acs.est.7b04232
Environ. Sci. Technol. 2017, 51, 13723−13732

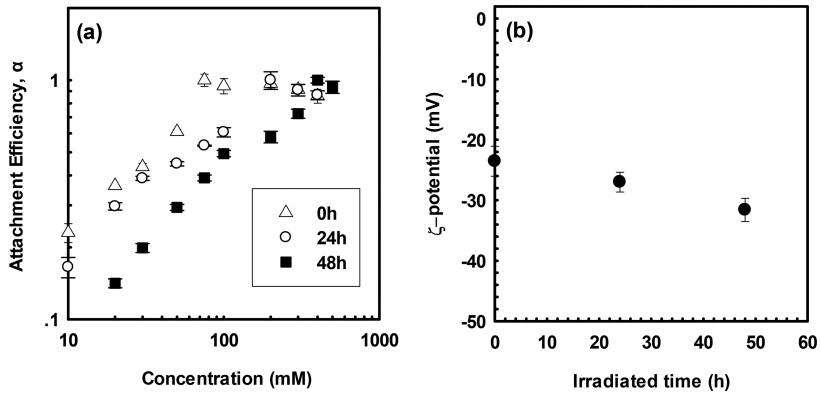

Figure 4. (a) Attachment efficiencies of original and irradiated DBC as a function of $CaCl_2$ concentration at pH 6.0 ± 0.4; (b) ζ-potential of original and irradiated DBC in deionized water. Error bar represents one standard deviation of five measurements.

efficiency α, ranging from 0 to 1, represents the probability of forming an aggregate during a collision between two DBC particles in the given water chemistry. It was determined by normalizing the initial aggregation rate in the solution of interest by that in the diffusion-limited regime.[25,26] Higher attachment efficiency suggests a less stable colloidal system. The attachment efficiencies of DBC in $CaCl_2$ and $BaCl_2$ solutions are summarized in Figure 3c and d. The stability plot has two distinct regimes. At low salt concentrations, the attachment efficiency increased with salt concentration. Then the attachment efficiency reached a plateau after the salt concentration exceeded the CCC. The CCC values for Ca^{2+} and Ba^{2+} are 75 mM and 60 mM, respectively. Overall, the destabilization capacity of the cations tested follows the order of $Ba^{2+} > Ca^{2+} \gg Mg^{2+}, Na^+$.

The electrokinetic properties of DBC in $MgCl_2$, $CaCl_2$, and $BaCl_2$ solutions are shown in Figure 2b. The ζ-potential of DBC became less negatively charged as salt concentration increased at the initial stage. Among the three divalent cations tested, the efficiency in reducing the surface potential of DBC follows $Ca^{2+} > Ba^{2+} > Mg^{2+}$ (Figure 2b), and they were all much more efficient in reducing the surface charge of DBC than monovalent ions. As the salt concentration further increased, charge reversal was observed in $CaCl_2$ and $BaCl_2$ solutions, which was in contrast to that in NaCl and $MgCl_2$ solutions and cannot be predicted by electric double layer models. The charge reversal concentration, c_R, (i.e., the concentration of electrolyte at the isoelectric point) was 150 mM for Ca^{2+} and 190 mM for Ba^{2+}. Charge reversal of particles and macromolecules was previously attributed to the formation of adsorbed layer of cationic polyelectrolytes, charge correlation effect, or specific sorption.[42−47] We hypothesize that Ca^{2+} and Ba^{2+} can specifically bond to DBC, which leads to the overcharging of the surface.

The drastically different aggregation and electrokinetic properties of DBC in Na^+, Mg^{2+}, Ca^{2+}, and Ba^{2+} solutions can be attributed to the different interaction mechanisms between cations and DBC. Na^+ is surrounded by a compact water shell in the aqueous phase and behaves as indifferent counterions that only affect the electrical double layer thickness. Thus, Na^+ has little impact on the hydrophilicity of DBC particles and consequently its aggregation behavior. Consistently, the ΔG^{AB} only slightly decreased from 37.3 mJ m^{-2} to 35.7 mJ m^{-2} as NaCl concentration increased from 10 mM to 800 mM. Mg^{2+} was reported to either form no complex with carboxyls in natural organic matter[48] or weak complexes.[49,50] It is also reported that the stability constants for complexes between Mg^{2+} and fulvic acids were much lower than that for Ca^{2+}.[51] The ΔG^{AB} decreased from 30.1 mJ m^{-2} to 9.8 mJ m^{-2} as $MgCl_2$ concentration increased from 10 mM to 800 mM. This decrease is more significant than that in NaCl solutions. Nevertheless, the energy barrier for aggregation was still high at 800 mM $MgCl_2$, 1.49×10^{-18} J (i.e., 368 k_BT, Figure 2d). Thus, Mg^{2+} also had limited impact on the aggregation behavior of DBC.

On the other hand, Ca^{2+} and Ba^{2+} were previously reported to form inner-sphere complexes with the carboxylic groups of humic substances.[48−50,52,53] The strong complexation between Ca^{2+}/Ba^{2+} and the oxygen-containing functional groups in DBC was consistent with the charge reversal observed (Figure 2b) and the XDLVO model calculation (Figure 3e and f). The ΔG^{AB} decreased to −4.6 mJ m^{-2} and −5.3 mJ m^{-2} in 100 mM $CaCl_2$ and $BaCl_2$ solutions receptively, indicating that the Lewis acid-base interactions shifted from repulsive (i.e., hydration force) to attractive (i.e., hydrophobic effect) at elevated Ca^{2+}/Ba^{2+} concentrations. Previous studies reported that highly charged biosurfaces changed from hydrophilic to hydrophobic as their charge was partially or completely neutralized by Ca^{2+}.[35,54,55] The complexation with Ca^{2+}/Ba^{2+} brings polar groups together, leading to a compact configuration of DBC. In this configuration, less polar groups but more hydrocarbon structures of DBC were exposed to the water phase, resulting in increased hydrophobicity.[54] This is consistent with the significantly reduced electron-donor surface tension component (γ^-) and the increased electron-acceptor surface tension component (γ^+) of DBC after the addition of Ca^{2+}/Ba^{2+} (Table S1). In addition, Ca^{2+} and Ba^{2+} can form complexes with carboxyl groups in different DBC particles, potentially leading to enhanced aggregation through bridging effect.[56]

Sunlight Exposure Increases the Colloidal Stability of DBC. The colloidal stability of DBC is closely related to its structural properties, which would determine its hydrophilicity and surface charge. Interactions with natural elements such as sunlight are expected to change the structure of DBC and consequently influence its colloidal stability. The aggregation profiles and electrokinetic properties of DBC before and after simulated sunlight exposure are compared in Figure 4. The colloidal stability of DBC in $CaCl_2$ solutions increased with irradiation time (Figure 4a). The CCC of the 48 h irradiated DBC was 400 mM, more than 5 times higher than that of the original DBC, 75 mM.

DOI: 10.1021/acs.est.7b04232
Environ. Sci. Technol. 2017, 51, 13723−13732

We investigated the structural evolution and hydrophilicity of DBC during irradiation using ^{1}H NMR. The ^{1}H NMR spectra were integrated over five regions: 0−1.2 ppm, methyl groups and unfunctionalized aliphatics; 1.2−1.9 ppm, aliphatic protons β and γ connected to keto or aromatic groups; 1.9−3.1 ppm, functionalized aliphatics, aliphatic protons α connected to keto or aromatic groups; 3.1−4.7 ppm, aliphatic protons connected to oxygen and nitrogen atoms; and 5.9−8.6 ppm, aromatic protons.[57,58] The percentages of protons in different moieties in DBC before and after irradiation from NMR analysis were summarized in Table 1.

Table 1. Composition of H Atoms in Different Moieties in DBC Obtained by ^{1}H-NMR

	0.0−1.2	1.2−1.9	1.9−3.1	3.1−4.7	5.9−8.6
moieties location (ppm)	methyl	aliphatic	functionalized aliphatic	heteroatom substituted	aromatic
original DBC	8.7	7.4	29.9	11.2	42.8
24 h-irradiated DBC	7.7	8.7	30.0	12.0	41.6
48 h-irradiated DBC	9.0	8.5	29.3	13.2	39.9

The aromatic protons decreased with increasing irradiation time from 42.8% to 39.9% after 48 h irradiation (Table 1), which was attributed to the substitution on aromatic rings and ring cleavage. On the other hand, the percentage of protons connected to oxygen and nitrogen atoms (i.e., heteroatom substituted H) increased from 11.2% to 13.2% after 48 h irradiation. As the formation of nitrogen-containing functional groups was expected to be minimal, the increase in the presence of these protons was attributed mostly to the oxidation processes that led to the formation of oxygen-containing functional groups. The percentage of aliphatic protons also increased, owing to the selective preservation and the generation of aliphatics during aromatic ring cleavage. Thus, DBC lost aromatic moieties but gained oxygen-containing and aliphatic moieties during sunlight exposure. This argument is in general consistent with a previous report using solid-state ^{13}C NMR technique.[3] Total aliphatics (including methyl, aliphatics, and functionalized aliphatics), which favor the hydrophobicity of DBC, grew 0.8% after 48 h. However, the loss of hydrophobic aromatic structures was more significant at 2.9%. DBC became more hydrophilic due to the loss of aromatic units and the addition of oxygen-containing moieties during irradiation, contributing to stronger hydration force. Meanwhile, the increase in oxygen-containing functional groups also leads to the increase in surface charge. The ζ-potential of DBC

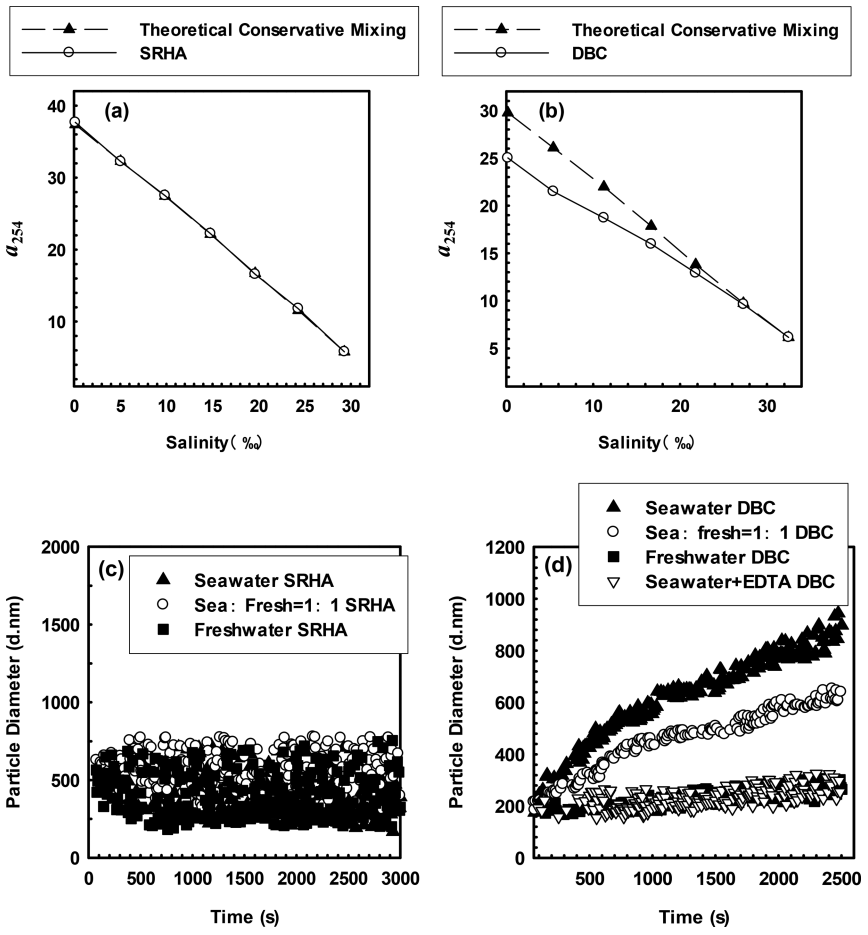

Figure 5. a_{254} as a function of the salinity for the mixture of seawater endmember and 10 mg/L (a) SRHA- or (b) DBC-containing freshwater endmember with different ratios after 24 h settling in dark condition at pH 7.7 ± 0.2 and 7.9 ± 0.2. The dashed line represents the theoretical conservative mixing line. The aggregation profile of (c) SRHA and (d) DBC in natural freshwater, seawater, their 1:1 mixture, and seawater with 13.68 mM EDTA at pH 7.0 ± 0.2 measured by time-resolved dynamic light scattering.

DOI: 10.1021/acs.est.7b04232
Environ. Sci. Technol. 2017, 51, 13723−13732

became more negative with irradiation time (Figure 4b). As a result, DBC samples with longer irradiation time underwent higher electrostatic repulsion and hydration force which facilitate their colloidal stability. The role of solar exposure on the aggregation behavior of DBC will be affected by the turbidity of the water which influences the number of photons received by DBC.

DBC in the Estuarine Mixing. The aggregation/sedimentation processes of DBC during Yangtze River Estuarine mixing were investigated by laboratory mixing experiments. The mixing curves for a_{254} of SRHA and DBC between two end-members, Yangtze River freshwater and East China Sea seawater, are presented in Figure 5a and 5b. The theoretical conservative mixing line represents the theoretical dilution scenario in which the DBC/SRHA concentration decreases linearly from 10 mg/L to ~0 mg/L with the mixing of water. It is a straight line connecting the two end-members. The mixing curve of SRHA coincided with the theoretical conservative mixing line as shown in Figure 5a, implying its conservative behavior during the mixing. The mixing curve of DBC was significantly below the theoretical dilution line, indicating the removal of DBC during the mixing (Figure 5b). The nonconservative behavior of DBC was observed over the entire salinity gradient including freshwater samples. The presence of 269 mg/L suspended particulate matter in the freshwater sample had limited impact on the sedimentation pattern of SRHA/DBC (SI Figure S3).

The nonconservative behavior of DBC in the laboratory mixing experiments can be attributed to its aggregation and sedimentation in the presence of Ca^{2+} and Ba^{2+}. The water chemistry of the natural water samples is summarized in SI Table S2. The aggregation profiles of SRHA and DBC in water samples collected from Yangtze River and the East China Sea, and their mixture are summarized in Figure 5c and d. The freshwater end-member contained 1.04 mM Ca^{2+} and no Ba^{2+}, and therefore was only able to induce slow aggregation of DBC (Figure 5d). The seawater end-member contained 12.82 mM Ca^{2+} and 0.09 mM Ba^{2+}, which led to fast aggregation of DBC (Figure 5d). Ca^{2+} is more important than Ba^{2+} due to its natural abundance. EDTA can effective chelate with Ca^{2+}, competing for their bonding with DBC. The addition of 13.68 mM EDTA to the seawater drastically inhibited the aggregation behavior of DBC (Figure 5d), further confirming the predominant role of Ca^{2+}. The aggregation kinetics increased with increasing seawater proportion which introduced more Ca^{2+} cations into the system. The aggregation behavior of DBC was also tested by sedimentation experiments in freshwater, seawater, and their mixture. The sedimentation rate increased with increasing seawater proportion (SI Figure S4), agrees with the aggregation kinetics. On the contrary, the size of SRHA remained unchanged in all the water samples within 50 min (Figure 5c). These results are consistent with their behavior in laboratory mixing experiments.

Environmental Implications. Our results suggest that the aggregation behavior of DBC is mainly controlled by the concentration of cations in aquatic systems that can complex with the polar functional groups in DBC, predominantly Ca^{2+} owing to its natural abundance. The electrokinetic properties commonly used for the prediction of colloidal stability, such as ζ-potential and electrophoretic mobility, do not apply for DBC as it is stabilized mainly through hydration force. Solar irradiation enhanced the colloidal stability of DBC in aquatic systems. Thus, the photoexposed DBC is expected to be more resistant to aggregation than that initially released from soils. Meanwhile, photodegradation processes were suggested to be one of the mechanisms for the loss of DBC in estuary waters.[59] Nevertheless, these effect is influenced by the light transmittance of the water column and will be hampered in high-turbidity waters. Results in this work imply that a portion of DBC flux will be transformed into the particulate matter by aggregation, leading to vertical mass flux in the estuaries. It is worth noting that the vertical mass flux of DBC is also expected in the freshwater systems based on our data. Thus, a portion of DBC released from the soil system, along with the contaminants associated, might accumulate in the riverine and estuarine sediments and will, therefore, be lost before it enters the oceans. The source material and combustion conditions will affect the properties and colloidal behavior of DBC. DBC with more hydrophilic structures is expected to have higher colloidal stability due to the predominant role of Lewis acid-base interactions. The structure−activity relationships for the colloidal stability of DBC should be addressed in future research. The different behavior of DBC and other DOM fractions in the fluvial and estuarine systems also may lead to the fractionation of DBC from the DOM pool, affecting the DBC/DOC ratio which is often assumed to be a stable characteristic for major rivers around the world and is used to estimate the global DBC flux.[5,22] Our results imply that this approach might lead to an overestimation of the land-ocean flux of DBC through fluvial transport as the DBC/DOC ratio will decrease along the salinity gradient due to the fractionation process. The significance of the fractionation process as well as riverine/estuarine sediments as a sink of DBC is unclear so far and needs further investigation at multiple scales.

■ ASSOCIATED CONTENT

Supporting Information

The Supporting Information is available free of charge on the ACS Publications website at DOI: 10.1021/acs.est.7b04232.

The experimental setup for irradiation experiments, the spectra of the xenon lamp and sunlight, TEM images of DBC particles, the lab mixing experiment with 269 mg/L suspended particulate matter, the calculation of the Lewis acid-base interaction energy (ΔG^{AB}), London-van der Waals force (ΔG^{LW}), electrostatic interaction energy (ΔG^{EDL}) of DBC in water, the contact angle and the surface tension data, sedimentation profiles of DBC in water samples, and water chemistry of the natural water samples (PDF)

■ AUTHOR INFORMATION

Corresponding Author

*Phone: +86-025-8968-0256; e-mail: xiaoleiqu@nju.edu.cn.

ORCID

Pedro J.J. Alvarez: 0000-0002-6725-7199
Qilin Li: 0000-0001-5756-3873
Xiaolei Qu: 0000-0002-9157-4274
Dongqiang Zhu: 0000-0001-6190-5522

Notes

The authors declare no competing financial interest.

■ ACKNOWLEDGMENTS

We thank Yuxuan Yao for her assistance in measuring DBC aggregation kinetics. This work was supported by the National

DOI: 10.1021/acs.est.7b04232
Environ. Sci. Technol. 2017, 51, 13723−13732

Key Basic Research Program of China (Grant 2014CB441103), the National Natural Science Foundation of China (Grant 21407073 and 21622703), the NSF ERC on Nanotechnology-Enabled Water Treatment (EEC-1449500), and the State Key Laboratory of Environmental Chemistry and Ecotoxicology, Research Center for Eco-Environmental Sciences, Chinese Academy of Sciences (KF2014-11).

REFERENCES

(1) Goldberg, E. *Black Carbon in the Environment*; Wiley and Sons: New York, NY, 1985.
(2) Dittmar, T.; de Rezende, C. E.; Manecki, M.; Niggemann, J.; Coelho Ovalle, A. R.; Stubbins, A.; Bernardes, M. C. Continuous flux of dissolved black carbon from a vanished tropical forest biome. *Nat. Geosci.* **2012**, *5*, 618−622.
(3) Fu, H.; Liu, H.; Mao, J.; Chu, W.; Li, Q.; Alvarez, P. J. J.; Qu, X.; Zhu, D. Photochemistry of dissolved black carbon released from biochar: Reactive oxygen species generation and phototransformation. *Environ. Sci. Technol.* **2016**, *50*, 1218−1226.
(4) Qu, X.; Fu, H.; Mao, J.; Ran, Y.; Zhang, D.; Zhu, D. Chemical and structural properties of dissolved black carbon released from biochars. *Carbon* **2016**, *96*, 759−767.
(5) Jaffe, R.; Ding, Y.; Niggemann, J.; Vahatalo, A. V.; Stubbins, A.; Spencer, R. G. M.; Campbell, J.; Dittmar, T. Global charcoal mobilization from soils via dissolution and riverine transport to the oceans. *Science* **2013**, *340*, 345−347.
(6) Dittmar, T.; Paeng, J. A heat-induced molecular signature in marine dissolved organic matter. *Nat. Geosci.* **2009**, *2*, 175−179.
(7) Hopkinson, C. S.; Vallino, J. J. Efficient export of carbon to the deep ocean through dissolved organic matter. *Nature* **2005**, *433*, 142−145.
(8) Santin, C.; Doerr, S. H.; Kane, E. S.; Masiello, C. A.; Ohlson, M.; Maria de la Rosa, J.; Preston, C. M.; Dittmar, T. Towards a global assessment of pyrogenic carbon from vegetation fires. *Global Change Biol.* **2016**, *22*, 76−91.
(9) McCarthy, J.; Zachara, J. ES&T features: Subsurface transport of contaminants. *Environ. Sci. Technol.* **1989**, *23*, 496−502.
(10) Wang, D. J.; Zhang, W.; Hao, X. Z.; Zhou, D. M. Transport of biochar particles in saturated granular media: Effects of pyrolysis temperature and particle size. *Environ. Sci. Technol.* **2013**, *47*, 821−828.
(11) Wang, D. J.; Zhang, W.; Zhou, D. M. Antagonistic effects of humic acid and iron oxyhydroxide grain-coating on biochar nanoparticle transport in saturated sand. *Environ. Sci. Technol.* **2013**, *47*, 5154−5161.
(12) Ward, C. P.; Sleighter, R. L.; Hatcher, P. G.; Cory, R. M. Insights into the complete and partial photooxidation of black carbon in surface waters. *Environ. Sci.-Process Impacts* **2014**, *16*, 721−731.
(13) Wagner, S.; Jaffe, R. Effect of photodegradation on molecular size distribution and quality of dissolved black carbon. *Org. Geochem.* **2015**, *86*, 1−4.
(14) Stubbins, A.; Niggemann, J.; Dittmar, T. Photo-lability of deep ocean dissolved black carbon. *Biogeosciences* **2012**, *9*, 1661−1670.
(15) Wells, M. L. Marine colloids: A neglected dimension. *Nature* **1998**, *391*, 530−531.
(16) Stedmon, C. A.; Markager, S. Behaviour of the optical properties of coloured dissolved organic matter under conservative mixing. *Estuarine, Coastal Shelf Sci.* **2003**, *57*, 973−979.
(17) Guo, W.; Stedmon, C. A.; Han, Y.; Wu, F.; Yu, X.; Hu, M. The conservative and non-conservative behavior of chromophoric dissolved organic matter in chinese estuarine waters. *Mar. Chem.* **2007**, *107*, 357−366.
(18) Mantoura, R. F. C.; Woodward, E. M. S. Conservative behaviour of riverine dissolved organic carbon in the severn estuary: Chemical and geochemical implications. *Geochim. Cosmochim. Acta* **1983**, *47*, 1293−1309.
(19) Yang, L. Y.; Guo, W. D.; Hong, H. S.; Wang, G. Z. Non-conservative behaviors of chromophoric dissolved organic matter in a turbid estuary: Roles of multiple biogeochemical processes. *Estuarine, Coastal Shelf Sci.* **2013**, *133*, 285−292.
(20) Benner, R.; Opsahl, S. Molecular indicators of the sources and transformations of dissolved organic matter in the Mississippi river plume. *Org. Geochem.* **2001**, *32*, 597−611.
(21) Yamashita, Y.; Jaffe, R.; Maie, N.; Tanoue, E. Assessing the dynamics of dissolved organic matter (DOM) in coastal environments by excitation emission matrix fluorescence and parallel factor analysis (EEM-PARAFAC). *Limnol. Oceanogr.* **2008**, *53*, 1900−1908.
(22) Stubbins, A.; Spencer, R.; Mann, P. J.; Holmes, R. M.; McClelland, J.; Niggemann, J.; Dittmar, T. Utilizing colored dissolved organic matter to derive dissolved black carbon export by arctic rivers. *Front. Earth Sci.* **2015**, *3*, 63.
(23) Yi, P.; Pignatello, J. J.; Uchimiya, M.; White, J. C. Heteroaggregation of cerium oxide nanoparticles and nanoparticles of pyrolyzed biomass. *Environ. Sci. Technol.* **2015**, *49*, 13294−13303.
(24) Brant, J. A.; Labille, J.; Bottero, J. Y.; Wiesner, M. R. Characterizing the impact of preparation method on fullerene cluster structure and chemistry. *Langmuir* **2006**, *22*, 3878−3885.
(25) Chen, K. L.; Elimelech, M. Aggregation and deposition kinetics of fullerene (C-60) nanoparticles. *Langmuir* **2006**, *22*, 10994−11001.
(26) Qu, X.; Hwang, Y. S.; Alvarez, P. J. J.; Bouchard, D.; Li, Q. UV irradiation and humic acid mediate aggregation of aqueous fullerene (nC60) nanoparticles. *Environ. Sci. Technol.* **2010**, *44*, 7821−7826.
(27) IHSS International humic substance society website. www.humicsubstances.org/.
(28) Kim, S. W.; Kaplan, L. A.; Benner, R.; Hatcher, P. G. Hydrogen-deficient molecules in natural riverine water samples - evidence for the existence of black carbon in DOM. *Mar. Chem.* **2004**, *92*, 225−234.
(29) Dittmar, T. The molecular level determination of black carbon in marine dissolved organic matter. *Org. Geochem.* **2008**, *39*, 396−407.
(30) Derjaguin, B.; Landau, L. Theory of stability of highly charged liophobic sols and adhesion of highly charged particles in solutions of electrolytes. *Prog. Surf. Sci.* **1945**, *15*, 663−682.
(31) Verwey, E. J. W. Theory of the stability of lyophobic colloids. *Philips Res. Repts.* **1945**, *1*, 33−49.
(32) Hotze, E. M.; Phenrat, T.; Lowry, G. V. Nanoparticle aggregation: Challenges to understanding transport and reactivity in the environment. *J. Environ. Qual.* **2010**, *39*, 1909−1924.
(33) Petosa, A. R.; Jaisi, D. P.; Quevedo, I. R.; Elimelech, M.; Tufenkji, N. Aggregation and deposition of engineered nanomaterials in aquatic environments: Role of physicochemical interactions. *Environ. Sci. Technol.* **2010**, *44*, 6532−6549.
(34) Chen, K. L.; Elimelech, M. Relating colloidal stability of fullerene (C60) nanoparticles to nanoparticle charge and electrokinetic properties. *Environ. Sci. Technol.* **2009**, *43*, 7270−7276.
(35) van Oss, C. J. Hydrophobicity of biosurfaces — origin, quantitative determination and interaction energies. *Colloids Surf., B* **1995**, *5*, 91−110.
(36) Zhang, Y.; Chen, Y.; Westerhoff, P.; Hristovski, K.; Crittenden, J. C. Stability of commercial metal oxide nanoparticles in water. *Water Res.* **2008**, *42*, 2204−2212.
(37) van Oss, C. J. Acid—base interfacial interactions in aqueous media. *Colloids Surf., A* **1993**, *78*, 1−49.
(38) Hardy, W. B. A preliminary investigation of the conditions which determine the stability of irreversible hydrosols. *Proc. R. Soc. London* **1900**, *66*, 110−125.
(39) Chin, W.-C.; Orellana, M. V.; Verdugo, P. Spontaneous assembly of marine dissolved organic matter into polymer gels. *Nature* **1998**, *391*, 568−572.
(40) Engebretson, R. R.; Amos, T. vonWandruszka, R., Quantitative approach to humic acid associations. *Environ. Sci. Technol.* **1996**, *30*, 990−997.
(41) Hsiao, P.-Y.; Luijten, E. Salt-induced collapse and reexpansion of highly charged flexible polyelectrolytes. *Phys. Rev. Lett.* **2006**, *97*, 148301.
(42) Besteman, K.; Van Eijk, K.; Lemay, S. G. Charge inversion accompanies DNA condensation by multivalent ions. *Nat. Phys.* **2007**, *3*, 641−644.

DOI: 10.1021/acs.est.7b04232
Environ. Sci. Technol. 2017, 51, 13723−13732

(43) Hierrezuelo, J.; Vaccaro, A.; Borkovec, M. Stability of negatively charged latex particles in the presence of a strong cationic polyelectrolyte at elevated ionic strengths. *J. Colloid Interface Sci.* **2010**, *347*, 202−208.
(44) Szilagyi, I.; Polomska, A.; Citherlet, D.; Sadeghpour, A.; Borkovec, M. Charging and aggregation of negatively charged colloidal latex particles in the presence of multivalent oligoamine cations. *J. Colloid Interface Sci.* **2013**, *392*, 34−41.
(45) Schneider, C.; Hanisch, M.; Wedel, B.; Jusufi, A.; Ballauff, M. Experimental study of electrostatically stabilized colloidal particles: Colloidal stability and charge reversal. *J. Colloid Interface Sci.* **2011**, *358*, 62−67.
(46) Lyklema, J. Overcharging, charge reversal: Chemistry or physics? *Colloids Surf., A* **2006**, *291*, 3−12.
(47) Borkovec, M.; Szilagyi, I.; Popa, I.; Finessi, M.; Sinha, P.; Maroni, P.; Papastavrou, G. Investigating forces between charged particles in the presence of oppositely charged polyelectrolytes with the multi-particle colloidal probe technique. *Adv. Colloid Interface Sci.* **2012**, *179−182*, 85−98.
(48) Kalinichev, A. G.; Kirkpatrick, R. J. Molecular dynamics simulation of cationic complexation with natural organic matter. *Eur. J. Soil Sci.* **2007**, *58*, 909−917.
(49) Ahn, W.-Y.; Kalinichev, A. G.; Clark, M. M. Effects of background cations on the fouling of polyethersulfone membranes by natural organic matter: Experimental and molecular modeling study. *J. Membr. Sci.* **2008**, *309*, 128−140.
(50) Iskrenova-Tchoukova, E.; Kalinichev, A. G.; Kirkpatrick, R. J. Metal cation complexation with natural organic matter in aqueous solutions: Molecular dynamics simulations and potentials of mean force. *Langmuir* **2010**, *26*, 15909−15919.
(51) Schnitzer, M.; Hansen, E. Organo-metallic interactions in soils: 8. An evaluation of methods for the determination of stability constants of metal-fulvic acid complexes. *Soil Sci.* **1970**, *109*, 333−340.
(52) Hering, J. G.; Morel, F. M. M. Humic-acid complexation of calcium and copper. *Environ. Sci. Technol.* **1988**, *22*, 1234−1237.
(53) Celebi, O.; Kilikli, A.; Erten, H. N. Sorption of radioactive cesium and barium ions onto solid humic acid. *J. Hazard. Mater.* **2009**, *168*, 695−703.
(54) Ohki, S. A mechanism of divalent ion-induced phosphatidylserine membrane fusion. *Biochim. Biophys. Acta, Biomembr.* **1982**, *689*, 1−11.
(55) Van Oss, C. J. Hydrophobic, hydrophilic and other interactions in epitope-paratope binding. *Mol. Immunol.* **1995**, *32*, 199−211.
(56) Kloster, N.; Brigante, M.; Zanini, G.; Avena, M. Aggregation kinetics of humic acids in the presence of calcium ions. *Colloids Surf., A* **2013**, *427*, 76−82.
(57) Schmitt-Kopplin, P.; Hertkorn, N.; Schulten, H. R.; Kettrup, A. Structural changes in a dissolved soil humic acid during photochemical degradation processes under O_2 and N_2 atmosphere. *Environ. Sci. Technol.* **1998**, *32*, 2531−2541.
(58) L. Malcolm, R. The uniqueness of humic substances in each of soil, stream and marine environments. *Anal. Chim. Acta* **1990**, *232*, 19−30.
(59) Stubbins, A.; Spencer, R. G. M.; Chen, H. M.; Hatcher, P. G.; Mopper, K.; Hernes, P. J.; Mwamba, V. L.; Mangangu, A. M.; Wabakanghanzi, J. N.; Six, J. Illuminated darkness: Molecular signatures of Congo river dissolved organic matter and its photochemical alteration as revealed by ultrahigh precision mass spectrometry. *Limnol. Oceanogr.* **2010**, *55*, 1467−1477.

DOI: 10.1021/acs.est.7b04232
Environ. Sci. Technol. 2017, 51, 13723−13732